BIOCHEMISTRY
including biophysical chemistry & molecular biology

Article

pubs.acs.org/biochemistry

Thermodynamics of Protein Self-Association and Unfolding. The Case of Apolipoprotein A-I

F. Zehender,[†] A. Ziegler,[†] H.-J. Schönfeld,[‡] and J. Seelig*,[†]

[†]Division of Biophysical Chemistry, Biozentrum, University of Basel, Klingelbergstrasse 50/70, CH-4056 Basel, Switzerland
[‡]Pharmaceutical Research, F. Hoffman-La Roche Ltd., CH-4070 Basel, Switzerland

ABSTRACT: Protein self-association and protein unfolding are two temperature-dependent processes whose understanding is of utmost importance for the development of biological pharmaceuticals because protein association may stabilize or destabilize protein structure and function. Here we present new theoretical and experimental methods for analyzing the thermodynamics of self-association and unfolding. We used isothermal dilution calorimetry and analytical ultracentrifugation to measure protein self-association and introduced binding partition functions to analyze the cooperative association equilibria. In a second type of experiment, we monitored thermal protein unfolding with differential scanning calorimetry and circular dichroism spectroscopy and used the Zimm−Bragg theory to analyze the unfolding process. For α-helical proteins, the cooperative Zimm−Bragg theory appears to be a powerful alternative to the classical two-state model. As a model protein, we chose highly purified human recombinant apolipoprotein A-I. Self-association of Apo A-I showed a maximum at 21 °C with an association constant K_a of 5.6×10^5 M^{-1}, a cooperativity parameter σ of 0.003, and a maximal association number n of 8. The association enthalpy was linearly dependent on temperature and changed from endothermic at low temperatures to exothermic above 21 °C with a molar heat capacity ΔC_p° of −2.76 kJ mol^{-1} K^{-1}. Above 45 °C, the association could no longer be measured because of the onset of unfolding. Unfolding occurred between 45 and 65 °C and was reversible and independent of protein concentration up to 160 μM. The midpoint of unfolding (T_0) as measured by DSC was 52−53 °C; the enthalpy of unfolding (ΔH_N^U) was 420 kJ/mol. The molar heat capacity ($\Delta_N^U C_p$) increased by 5.0 ± 0.5 kJ mol^{-1} K^{-1} upon unfolding corresponding to a loss of 80−85 helical segments, which was confirmed by circular dichroism spectroscopy. Unfolding was highly cooperative with a nucleation parameter σ of 4.4×10^{-5}.

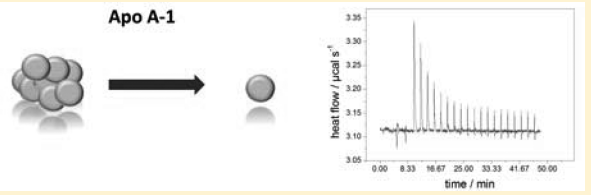

In situ, biological molecules are confronted with a spectrum of structures, concentrations, ions, etc., a situation thermodynamically distinct from that of dilute solutions in vitro. Macromolecular crowding may lead to nonspecific homo- or heteroassociation, and an understanding of functional mechanisms requires quantitative analysis of protein association equilibria. The thermodynamic treatment of coupled reactions with many intermediates is a complex process, as temperature changes influence both the association equilibrium and protein stability. Here we consider protein association and protein unfolding as two independent cooperative processes. The protein association−dissociation equilibrium is described as a multistate process using binding partition functions. Protein unfolding is analyzed with the nearest-neighbor Zimm−Bragg theory and compared to the classical two-state N ⇄ U model. We apply these theoretical models to experimental data obtained with apolipoprotein A-I (Apo A-I).

Apo A-I, a 28.2 kDa protein, reduces cardiovascular risks by promoting the reverse transport and metabolism of cholesterol. Its structural and functional properties with and without lipid have been intensively investigated (for reviews, see refs 1 and 2). X-ray diffraction and circular dichroism (CD) spectroscopy demonstrate that Apo A-I contains long stretches of α-helical structure.[3−8] α-Helix is enhanced after lipid binding.[9] Analysis of the thermodynamics of lipid binding reveals that the association number[10] and lipid-to-protein ratio[11] markedly influence the shape of reconstituted particles, suggestive of functional differences. The association equilibrium of lipid-free Apo A-I is, however, an area of ambiguity with diverging reports about its association number and association mechanism (for a recent survey, see ref 12).

We investigated the variability mentioned above with highly purified recombinant human Apo A-I. The monomer−oligomer equilibrium was investigated with high-sensitivity titration calorimetry (ITC). By diluting concentrated Apo A-I solutions in the calorimeter cell, we were able to determine the association enthalpy, ΔH_a°, association constant, K_a, and association number, n, of oligomer formation as a function of temperature. Sedimentation equilibrium runs in the analytical ultracentrifuge (AUC) provided an independent approach to elucidating the association constant and stoichiometry. We propose a cooperative association model and develop analytical expressions for the degree of dissociation and molar heat capacity change upon oligomer dissociation.

CD spectra were recorded as a function of protein concentration and temperature to monitor structural changes. Differential scanning calorimetry was used to quantify the

Received: September 1, 2011
Revised: January 20, 2012
Published: January 23, 2012

thermodynamics of protein unfolding. Taking into account changes in molar heat capacity upon unfolding and using the cooperative Zimm–Bragg model for α-helix–coil transitions, we were able to correlate structural changes observed by CD spectroscopy with thermodynamic DSC data. Apo A-I unfolding was found to thermodynamically override Apo A-I association.

MATERIALS AND METHODS

Proteins. A detailed protocol for the medium scale preparation of recombinant human Apo A-I will be published separately (H.-J. Schönfeld et al., manuscript in preparation). Briefly, a fusion protein construct involving a hexahistidine purification tag, a ubiquitin sequence, a Granzyme B cleavage site (IEPD|GG) and the human Apo A-I sequence (N- to C-terminus) was recombinantly expressed in *Escherichia coli*.

After the cells had been opened by being subjected to French press treatment, the recombinant fusion protein was bound to a Ni-NTA column and then washed with alternating cycles of two buffers, one containing 8 M urea and the other containing 60% 2-propanol, to remove bacterial endotoxins. The fusion protein was eluted using EDTA and cleaved with Granzyme B, and the hexahistidine tag containing the N-terminus was removed from the mixture by a second Ni-NTA affinity step. Recombinant protein that did not bind to Ni-NTA contained the authentic human Apo A-I sequence with two additional glycines at the N-terminus. The Apo A-I protein was further purified by anion exchange chromatography and then extensively dialyzed against phosphate-buffered saline (PBS). Purified Apo A-I contained no significant amount of aggregates as analyzed by size exclusion chromatography with online static light scattering and no detectable endotoxins as measured by a limulus assay. The purified recombinant Apo A-I sequence differed from the human wild-type (wt) Apo A-I sequence by two additional N-terminal glycine residues. Electrospray mass spectrometry revealed a molecular mass of 28192.3 Da (the theoretical value for wt Apo A-I with two Gly residues is 28192.7 Da). Comparison by size exclusion chromatography (data not shown) and analytical ultracentrifugation (Figure 3C) did not reveal any differences in higher-order structure between recombinant Apo A-I and Apo A-I purified from human plasma, a generous gift from T. Tetaz (Roche, Basel, Switzerland).

Circular Dichroism (CD) Spectroscopy. CD spectra were recorded with a model 62 ADS CD spectrometer (AVIV, Lakewood, NJ) in the wavelength range from 190 to 260 nm using a total acquisition time of 25 min per spectrum. Measurements were taken with protein concentrations of 0.1 and 0.5 mg/mL in 100 mM NaF and 10 mM sodium phosphate (pH 7.4). Quartz cuvettes with path lengths (d) of 1 and 0.2 mm were used, and a baseline with pure buffer was recorded for each cuvette and subtracted from the protein spectra. The CD spectra were simulated with the noncommercial software CDpro[13] on the basis of reference spectra of 56 proteins (data set 10) and also with an Excel program on the basis of a linear combination of reference spectra.[14] The melting behavior of Apo A-I was studied in the range of 25–85 °C.

High-Sensitivity Isothermal Titration Calorimetry (ITC). ITC was performed using either the ITC-200 or the VP titration calorimeter from Microcal (Northampton, MA). The cell volumes were 200 μL and 1.4 mL, respectively, and the injection volume varied between 2 and 10 μL. Solutions were degassed under vacuum for ~10 min. The calorimeter cell contained buffer, and the protein solution (80 or 160 μM) was in the injection syringe. The injection of small amounts of a concentrated Apo A-I solution into buffer led to the dissociation of Apo A-I complexes. The heat flow induced by protein dissociation was recorded and analyzed by the software provided with the instrument. The quantitative interpretation of the Apo A-I dissociation isotherm in terms of thermodynamic parameters was not part of the commercial software and is discussed below. All measurements were taken in PBS buffer [137 mM NaCl, 10 mM sodium phosphate (pH 7.4), and 0.02% NaN_3].

Differential Scanning Calorimetry (DSC). DSC scans were made with a VP-DSC instrument (Microcal). Protein solutions were degassed, and the reference cell contained only buffer. The heating rate was 1 °C/min. DSC scans were made in PBS buffer (pH 7.4) with 0.02% NaN_3. Further evaluation of the DSC curves was performed as described in Results.

Analytical Ultracentrifugation (AUC). A Beckman XL-I ultracentrifuge (Beckman Coulter, Indianapolis, IN) with UV and interference detection systems was used. Protein solutions were measured in PBS buffer at concentrations from 0.5 to 2 mg/mL with 0.02% NaN_3. Sedimentation velocity (SV) and sedimentation equilibrium (SE) measurements were taken at 20 °C. Depending on the protein concentration, the centerpiece length was 1.4, 3, or 12 mm. Rotational speeds in SE runs were between 5K and 18K rpm. Using a liquid column height of ~5 mm, equilibria were reached within ~68 h, as verified by comparison with subsequent radial scans.

THEORY

Analysis of Calorimetric Protein Unfolding Experiments. The calorimetric enthalpy of the N ⇄ U unfolding process is temperature-dependent and can be calculated by

$$\Delta_N^U H(T) = f_U(T)[\Delta H^\circ + \Delta_N^U C_p(T - T_0)] \quad (1)$$

where $f_U = (1 - f_N)$ is the fraction of unfolded protein ($0 \le f_U \le 1$), ΔH° is the unfolding enthalpy, $\Delta_N^U C_p$ is the difference in the molar heat capacity between the native and unfolded protein, and T_0 is a reference temperature, usually the midpoint of the unfolding curve. The heat capacity change measured in the DSC calorimeter is given by

$$\Delta_N^U C_p(T) = f_U(T)\Delta_N^U C_p + [\Delta H^\circ + \Delta_N^U C_p(T - T_0)]\frac{df_U(T)}{dT} \quad (2)$$

In the following, we use two models to calculate the extent of unfolding f_U.

The classical model for protein unfolding is the N ⇄ U two-state model. The fraction of unfolded protein is related to the temperature-dependent equilibrium constant $K_N^U(T) = [U]/[N]$ according to

$$f_U(T) = \frac{K_N^U(T)}{1 + K_N^U(T)} \quad (3)$$

At the midpoint T_0 of the transition, the enthalpy and entropy are equal. The free energy change of unfolding, $\Delta_N^U G(T)$, can be written

$$\Delta_N^U G(T) = \Delta H^\circ\left(1 - \frac{T}{T_0}\right) + \Delta_N^U C_p\left(T - T_0 + \ln\frac{T}{T_0}\right) \quad (4)$$

dx.doi.org/10.1021/bi2013799 | *Biochemistry* 2012, 51, 1269–1280

The temperature dependence of the equilibrium constant is given by

$$K_N^U(T) = e^{-\Delta_N^U G(T)/RT} \quad (5)$$

The three independent parameters that need to be determined are ΔH°, $\Delta_N^U C_p$, and T_0. T_0 designates the midpoint of the N ⇄ U transition where $\Delta_N^U G(T_0) = 0$ and $K_N^U(T_0) = 1$. ΔH° is the van't Hoff enthalpy of the transition and must be distinguished from the calorimetric enthalpy ΔH_{cal}, which is measured with the DSC instrument. In an ideal fit of the N ⇄ U model, the two quantities are identical. However, if ΔH° and ΔH_{cal} are different, the deviation of $\Delta H^\circ/\Delta H_{cal}$ from unity is considered to be indicative of intermediates in the transition. The calorimetric curve is then approximated by a superposition of several N ⇄ U transitions.

The N ⇄ U model does not completely reveal the molecular aspects of protein unfolding. However, many proteins, such as Apo A-I, have a high α-helix content, and a specific molecular process of unfolding is the cooperative "melting" of the α-helix. We therefore propose an alternative description of Apo A-I unfolding in terms of the cooperative α-helix ⇄ random coil transition, and we will extend this model to include β-structure formation. The degree of unfolding, $f_U(T)$, is calculated with the Zimm–Bragg matrix method[15] and combined with eqs 1 and 2. The Zimm–Bragg model considers the α-helix ⇄ random coil transition as the cooperative disruption of n hydrogen bonds. It is an enthalpy-driven process, and the enthalpy change in breaking a single helical hydrogen bond (h) is in the range of 3.8 kJ/mol (0.9 kcal/mol) to 5.4 kJ/mol (1.3 kcal/mol).[16−18] While h itself is independent of temperature, the temperature dependence of the equilibrium constant $s(T)$ (growth parameter) follows van't Hoff's law according to

$$s(T) = e^{h/R(\frac{1}{T} - \frac{1}{T_1})} \quad (6)$$

At T_1, the growth parameter s is $s(T_1) = 1$. T_1 defines the midpoint of the α-helix ⇄ random coil transition for a sufficiently long and highly cooperative polypeptide chain. Under these conditions, T_1 is identical with the experimentally observed midpoint T_0. However, chain length n has a dramatic effect on the melting behavior. Short chains melt at lower temperatures than long chains, and the theory then predicts the midpoint temperature T_0 at temperatures lower than T_1.

The second parameter in Zimm–Bragg theory is nucleation factor σ, which is related to the probability of forming an α-helix nucleus within a random coil sequence. σ determines the cooperativity of the system and is assumed to be temperature-independent.

Zimm–Bragg theory defines conditional probabilities for extending a given peptide chain by one additional segment, where "segment" is identical to a single amino acid in the protein sequence. Adding a helix segment to an existing α-helix requires the growth parameter s; formation of an α-helix nucleus within a random coil sequence is defined by the nucleation parameter σs. The occurrence of a coil segment has a probability of 1. In the nearest neighbor approximation, these conditional probabilities can be summarized in the probability matrix $\mathbf{M}$.[15,19]

$$\mathbf{M} = \begin{pmatrix} 1 & 1 \\ \sigma s & s \end{pmatrix} \quad (7)$$

The partition function of a chain of n segments is then given by

$$Z = (1 \quad 1)\mathbf{M}^n \begin{pmatrix} 1 \\ 0 \end{pmatrix} \quad (8)$$

Knowledge of the partition function allows the calculation of the α-helix fraction according to

$$f_h = \frac{1}{n}\frac{\partial \ln Z}{\partial s} \quad (9)$$

As s is a function of temperature, $\mathbf{M}$, Z, and f_h are equally temperature-dependent. The fraction of unfolded protein is

$$f_U(T) = 1 - f_h \quad (10)$$

$f_U(T)$ can then be combined with eq 2 to calculate $\Delta_N^U C_p(T)$.

A convenient approach to calculating the helix fraction is eq 27 of ref 15, which can easily be programmed.

Association–Dissociation Equilibrium of Apo A-I. The association of Apo A-I is a separate process that must be distinguished from unfolding. It is described here by a chemical model that includes cooperativity and growth and has been applied successfully in describing surfactant association in micelles.[20]

$$A + A \rightarrow A_2;\ A_2 + A \rightarrow A_3;\ \ldots \rightarrow A_n$$

The formation of the dimer (A + A ⇄ A_2) is the nucleation step

$$c_{A_2} = \sigma K_a {c_A}^2 \quad (11)$$

which is followed by several growth steps

$$c_{A_3} = K_a c_{A_2} c_A = \sigma {K_a}^2 {c_A}^3 \quad (12)$$

$$c_{A_n} = K_a c_{A_{n-1}} c_A \quad (13)$$

σ is the nucleation parameter (different from that of Zimm–Bragg theory) and c_A is the monomer equilibrium concentration. The equilibrium constant K_a is temperature-dependent according to van't Hoff's law. The corresponding enthalpy of association, ΔH_a°, is also temperature-dependent and is written as

$$\Delta H_a^\circ(T) = \Delta H_a^\circ + \Delta C_{p,a}^\circ (T - T_0) \quad (14)$$

T_0 is an arbitrary reference temperature. $\Delta C_{p,a}^\circ$ is the molar heat capacity change of the association reaction. All numerical values refer to protein monomers.

If c_A^0 is the total concentration of monomer A and $q = K_a c_A$, defined as the growth parameter, mass conservation requires

$$c_A^0 = c_A\left(1 + \sigma \sum_{j=2}^{n} j q^{j-1}\right) \quad (15)$$

We introduce a binding partition function Q that represents the sum of all concentrations found in the system referenced to the monomer concentration c_A (cf. ref 21)

$$c_A + c_{A_2} + \ldots c_{A_n} = c_A\left(1 + \sigma \sum_{j=2}^{n} q^{j-1}\right) = c_A Q \quad (16)$$

$$Q = 1 + \sigma \sum_{j=2}^{n} q^{j-1} = 1 + \frac{\sigma(q - q^N)}{1 - q} \quad (17)$$

dx.doi.org/10.1021/bi2013799 | Biochemistry 2012, 51, 1269–1280

The degree of dissociation (fraction of monomers) at a given total concentration, c_A^0, is given by

$$\alpha = \frac{c_A}{c_A^0} \tag{18}$$

and can be calculated as

$$\alpha = \left(q\frac{\partial Q}{\partial q} + Q\right)^{-1} \tag{19}$$

The temperature dependence of α is given by

$$\frac{d\alpha}{dT} = qQ^*\frac{\Delta H_a^\circ(T)}{RT^2}\left(-\frac{1}{\alpha^2} - QK_a c_A^0\right)^{-1} \tag{20}$$

where

$$Q^* = 2\frac{\partial Q}{\partial q} + q\frac{\partial^2 Q}{\partial q^2} \tag{21}$$

We now consider a thought experiment in which the protein is locked in its native conformation and a change in temperature influences only the association equilibrium but not the protein conformation. If this experiment is performed in the DSC instrument, the molar heat capacity change is predicted as

$$\Delta C_{p,a}(T) = \Delta C_{p,a}^0\alpha + \Delta H_a(T)\frac{d\alpha}{dT} \tag{22}$$

Knowing the temperature dependence of ΔH_a and K_a, we can predict the degree of dissociation, α, and the molar heat capacity change, $\Delta C_{p,a}$.

For the sake of completeness, we mention two alternative association models that are discussed in the literature in connection with Apo A-I. The first is the all-or-none model

$$nA \rightleftarrows A_n \tag{23}$$

which can be described by

$$c_{A_n}/{c_A}^n = {K_a}^{n-1} \tag{24}$$

Defining again

$$q = c_A K_a \tag{25}$$

this leads to the binding partition function

$$Q = 1 + q^{n-1} \tag{26}$$

where the degree of dissociation can again be calculated with eq 19.

The second model suggests a monomer−dimer−tetramer−hexamer−octamer equilibrium.[22] In our notation, the binding partition function of this model is given by

$$Q(n) = 1 + \sigma\sum_{j=1}^{n-1} q^{2j-1} = 1 + \sigma\frac{q - q^{2n-1}}{1 - q^2} \tag{27}$$

The nucleation parameter is included for generality and must be defined as $\sigma = 1$ to make eq 27 equivalent to the model of ref 22 mentioned above. Again eq 19 can be used to derive the degree of dissociation α.

RESULTS

Isothermal Titration Calorimetry (ITC) of the Apo A-I Monomer ⇄ Oligomer Equilibrium. Apo A-I self-associates in solution even at low protein concentrations,[12,22,23] but thermodynamic aspects of Apo A-I self-association have not yet been investigated in detail. The availability of high-sensitivity titration calorimetry now permits the deduction of the enthalpy of association, ΔH_a, the binding constant, K_a, and the association number, n, from dilution experiments. The calorimetric titration sequence is analogous to that used in detergent demicellization experiments to determine the critical micellar concentration.[20,24] In this study, the dilution involves oligomers of different sizes and the stoichiometry is not known. Also not known is the effect of temperature on the association−dissociation equilibrium.

Figure 1A displays the heat flow in a dilution experiment in which Apo A-I (160 μM) was injected into PBS buffer. At 40 °C, the heat of dissociation was endothermic but changed to exothermic when the experiment was performed below 20 °C.

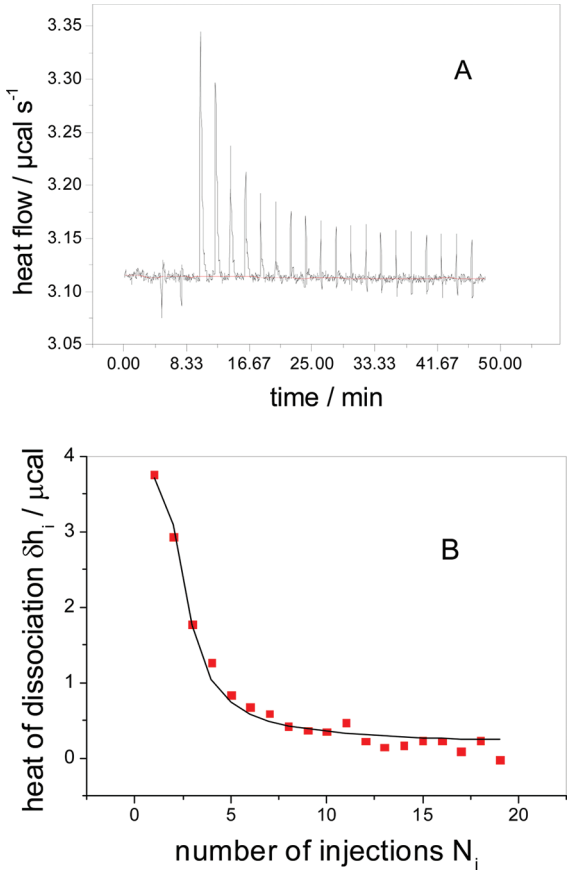

Figure 1. Dissociation reaction of Apo A-I measured via isothermal titration calorimetry (ITC). (A) Heat flow. A 160 μM solution of Apo A-I in PBS buffer [138 mM NaCl, 10 mM sodium phosphate (pH 7.4), and 0.02% NaN_3] was injected as 2 μL aliquots into the calorimeter cell (V_{cell} = 0.2 mL) containing only buffer. The heat of reaction, δh_i, arises from the dissociation reaction of Apo A-I oligomers as each injection corresponds to an ∼100-fold dilution of protein concentration. The measurement was taken at 40 °C. At room temperature, the heat of dissociation is close to zero and the dissociation reaction cannot be detected by ITC. (B) Integrated heats of reaction, δh_i, as a function of injection number. The solid line shows the theoretical analysis based on the cooperative association model. The maximal association number n = 8. The association constant K_a (40 °C) = 3.5 × 10^5 M^{-1}. σ = 0.003. The measured heat of dissociation ΔH = 49.1 kJ/mol (11.74 kcal/mol). The corrected heat of dissociation was 51.3 kJ/mol (12.3 kcal/mol) as the starting solution contained 4.4% monomers.

dx.doi.org/10.1021/bi2013799 | Biochemistry 2012, 51, 1269−1280

Table 1. Thermodynamic Parameters of the Apo A-I Self-Association Equilibrium Calculated with the Cooperative Association Model

			maximal association number n = 8				
temp (°C)	$c_{\text{Apo A-I}}$ (μM)	ΔH^a (kcal/mol)	$\Delta H_a^{\circ b}$ (kcal/mol)	σ	K_a (M^{-1})	ΔG_a° (kcal/mol)	$T\Delta S_a^\circ$ (kcal/mol)
5	160	−7.7	8.14	0.003	2.8×10^5	−6.90	15.04
5	160	−8.51	9.03	0.003	2.6×10^5	−6.86	15.89
10	160	−6.95	7.19	0.003	4.8×10^5	−7.33	14.52
10	160	−7.03	7.31	0.003	4.0×10^5	−7.23	14.55
35	160	7.34	−7.59	0.003	4.9×10^5	−7.99	0.40
40	80	9.22	−10.1	0.003	3.3×10^5	−7.87	−2.20
40	160	11.74	−12.3	0.003	3.5×10^5	−7.91	−4.37
45	160	18.5	−19.8	0.003	2.4×10^5	−7.80	−11.99

[a] ΔH is the heat of dissociation as measured in the calorimetric experiment. While the precision of an individual calorimetric measurement is high (±0.2 kcal/mol), the reproducibility is determined by different factors and is on the order of ±1.3 kcal/mol. [b] ΔH_a° is the enthalpy of protein association; $\Delta H_a^\circ = -\Delta H/(1-\alpha)$, where α is the fraction of monomers in the starting solution.

Integration of the calorimetric response peaks yielded the heats of reaction, δh_i (Figure 1B). The first protein injection corresponded to a >100-fold dilution of the starting solution and resulted in a complete dissociation of the Apo A-I complex. The molar heat of dissociation is then given by

$$\Delta H = \frac{\delta h_1}{\delta n} \tag{28}$$

where δh_1 is the measured heat of dissociation of the first injection and δn is the molar amount of injected Apo A-I.

However, the experimentally derived ΔH is not the full molar heat of dissociation, ΔH_D°. The thermodynamic and statistical analysis discussed below shows that the 160 μM Apo A-I solution is composed of Apo A-I complexes (~95%) and a small fraction of monomers (~5%). The true heat of dissociation, ΔH_D° is thus larger than the measured value of ΔH. The correct value follows from the theoretical analysis of the dissociation isotherm as described in more detail below. Table 1 shows the measured ΔH and the corrected heat of association ($\Delta H_a^\circ = -\Delta H_D^\circ$). ΔH_a° has the opposite sign of the heat of dissociation. When the fraction of monomers, α, is taken into account, ΔH_a° is given by

$$\Delta H_a^\circ = -\Delta H/(1-\alpha) \tag{29}$$

Continued addition of Apo A-I to the calorimeter cell causes dissociation to stop. The degree of dissociation, α_i, after i injections is given by

$$\alpha_i = \frac{\sum_i \delta h_i}{i\delta h_1} \tag{30}$$

The nominator is the cumulative heat measured for the first i injections, and the denominator is the predicted maximum heat, $i \times \delta h_1$, expected for complete dissociation after i injections. The ITC dilution experiment thus provides both the dissociation enthalpy, ΔH_D°, and the dissociation isotherm $\alpha = f(c_p^0)$. c_p^0 is the total concentration of protein in the calorimeter cell and increases with each injection.

ITC measurements were performed between 5 and 45 °C, and Figure 2A displays the temperature dependence of the association enthalpy ΔH_D°. The enthalpy changes its sign at ~20 °C, and the slope of the straight line yields the molar heat capacity change for the association reaction as $\Delta C_p^\circ = -2.76$ kJ mol^{-1} K^{-1} (−0.66 kcal mol^{-1} K^{-1}). Apo A-I self-association is thermodynamically similar to the partitioning of hydrophobic substances between water and an organic phase.[25]

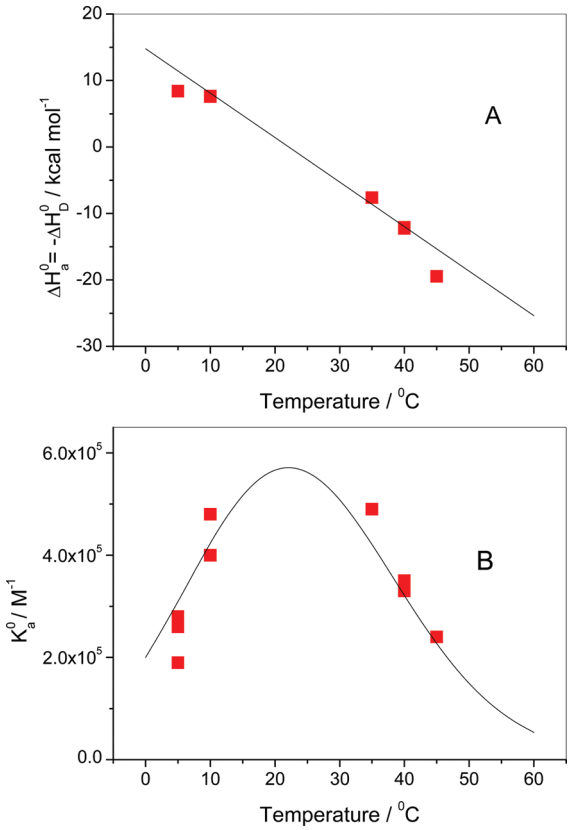

Figure 2. Thermodynamic parameters of Apo A-I self-association. (A) Enthalpy, ΔH_a°, of Apo A-I self-association as determined via isothermal titration calorimetry. (B) Temperature dependence of association constant K_a. K_a was calculated by fitting the dilution isotherms of the calorimetric titration experiments with the cooperative association model using an n of 8 and a σ of 0.003. The solid line predicts the temperature dependence of K_a by combining the van't Hoff equation with the temperature-dependent ΔH_a° of panel A.

The enthalpy of dissolving hydrophobic substances such as hexane in water is close to zero at room temperature, while the heat capacity increment for the transfer from water into the pure organic phase is large and negative. Apo A-I self-association paralleled this behavior, as the enthalpy of Apo A-I self-association was zero at room temperature and the heat capacity change strongly negative. Calorimetric experiments at 15−30 °C were not feasible because $\Delta H_a^\circ \sim 0$ kcal/mol.

dx.doi.org/10.1021/bi2013799 | Biochemistry 2012, 51, 1269−1280

Apo A-I dissociation as measured by ITC was analyzed with the cooperative association model. The result is shown in Figure 1B (solid line), which simulates the dilution measurement at 40 °C and was calculated with an association constant K_a of 3.5 × 10^5 M^{-1}, a nucleation factor σ of 0.003, and a maximal association number n of 8. An excellent fit between theory and experiment was obtained.

The cooperative model was further applied to investigate the influence of association number n on the quality of the simulation. A minimal n of 6 was required to generate a good fit of the ITC data over the whole temperature range. An increase in n from 6 to 20 provided simulations of similar quality but reduced the values of nucleation parameter σ and association constant K_a. At n = 20, a "plateau" was reached where an increase in n had no further effect on σ or K_a. However, analytical ultracentrifugation data discussed below argue against an association number larger than 8.

Figure 2B shows the temperature dependence of Apo A-I association constant K_a (addition of a monomer to an existing complex) when n = 8. The solid line is the predicted temperature dependence of K_a calculated with the van't Hoff equation and a temperature-dependent ΔH_a° (Figure 2A). The simulations also showed that a nucleation parameter σ of $\ll$1 was essential for the correct interpretation of the experimental data. Initial dimer formation is thermodynamically less favored than the addition of monomers to an existing complex.

As an alternative model, we also evaluated the all-or-none model. A fit of the ITC data was possible with an n of 6. However, the model assumes only monomers and hexamers without intermediates, is kinetically impossible, and disagrees with the results of analytical ultracentrifugation.

Analytical Ultracentrifugation Analysis of Apo A-I Self-Association. Previous studies of Apo A-I self-association used AUC measurements of serum-purified Apo A-I.[22,26] We therefore compared the recombinant Apo A-I (with two additional C-terminal glycines) used in this study with serum-purified Apo A-I also using AUC. Figure 3A shows sedimentation equilibrium runs at 6K, 8K, and 10K rpm for recombinant Apo A-I (160 μM) in PBS buffer. The protein concentration increases with an increasing radius r, and thus, each point in the concentration, c, versus radius, r, profile corresponds to a different equilibrium between monomers and Apo A-I complexes. Quantitative analysis is possible via calculation of both the total Apo A-I concentration at a given radius r and the slope of the ln(c) versus r^2 curve at the same position. We determined local slopes of the ln(c) versus r^2 function by linearizing 8−10 consecutive data points, computing the slope of this linearized interval, and then shifting the interval to the next data point. Figure 3B shows the apparent molecular mass, M_{app}, as a function of the corresponding total Apo A-I concentration. We assumed that monomeric and oligomeric Apo A-I molecules have the same specific optical absorption at 280 nm. Figure 3B summarizes data obtained for Apo A-I solutions at initial concentrations of 3, 40, and 160 μM measured at six different rotor speeds between 4K and 15K rpm. Data scatter is considerable, but the semilogarithmic plot clearly shows a horizontal lag phase up to ~3 μM where no association occurs and where M_{app} is identical to the molecular mass of monomeric Apo A-I. Above 3 μM, M_{app} increases sigmoidially. The solid line in Figure 3B corresponds to the best fit using the cooperative model with a K_a of 3.5 × 10^5 M^{-1}, an n of 8, and a σ of 0.003. Calorimetric measurements yielded a K_a of 5.6 × 10^5 M^{-1} at 20 °C (represented by the dashed line in Figure 3B), indicating good agreement between AUC and ITC. The nucleation parameter σ determines the length of the monomeric lag phase as well as the steepness of the transition curve.

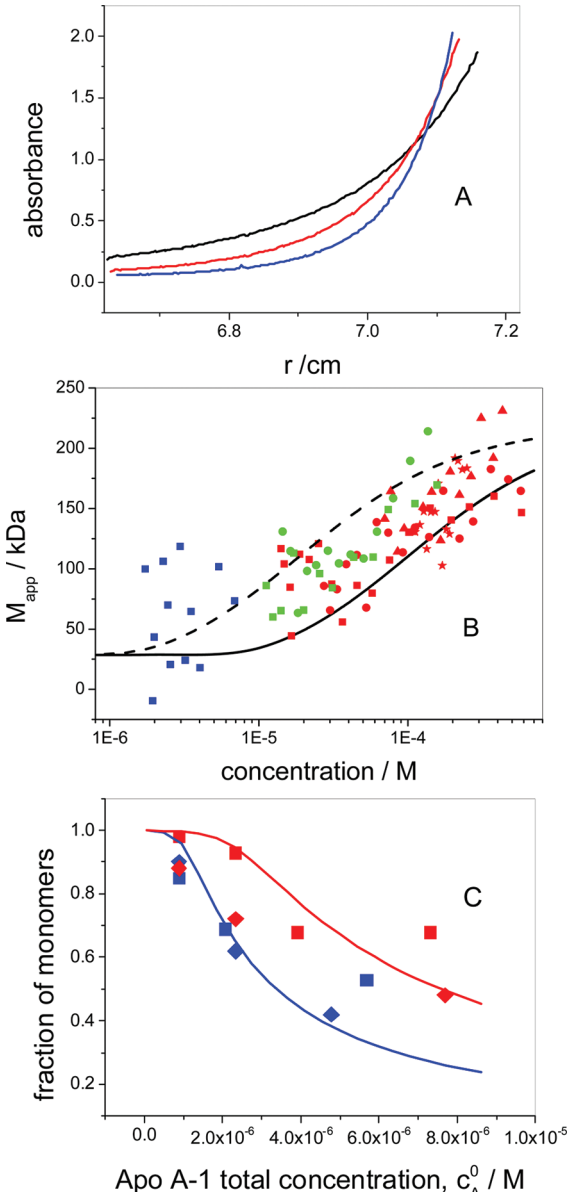

Figure 3. Apo A-I self-association measured via analytical ultracentrifugation (AUC). (A) Sedimentation equilibrium experiments. Apo A-I at a concentration of 160 μM in PBS buffer was centrifuged for 96 h at 6K (black), 8K (red), and 10K rpm (blue) at 20 °C. (B) Apparent molecular mass, M_{app}, as a function of total Apo A-I concentration. Three concentrations were simultaneously measured: 3 μM (blue data points, cuvette size of 12 mm), 40 μM (green data points, cuvette size of 3 mm), and 160 μM (red data points, cuvette size of 1.4 mm). Measurements were taken at 6K (■), 8K (▲), 10K (♦), 12K (●), and 15K rpm (★). Analyses were limited to a maximal optical density (OD) of 2. The solid line was calculated with the cooperative association model using the following values: n = 8, σ = 0.003, and K_a = 3.5 × 10^5 M^{-1}. The dashed line corresponds to a K_a of 5.6 × 10^5 M^{-1} predicted by ITC at 20 °C. (C) Degree of dissociation, α, as a function of total protein concentration. Recombinant Apo A-I (■) is compared with serum-purified Apo A-I (♦). Measurements were taken at 20 °C (blue points) and 37 °C (red points). The solid lines are the predictions of the cooperative association model with the following values: n = 8, σ = 0.003, and K_a = 4.0 × 10^5 M^{-1} (37 °C, red line) or K_a = 8 × 10^5 M^{-1} (20 °C, blue line).

dx.doi.org/10.1021/bi2013799 | Biochemistry 2012, 51, 1269−1280

Figure 3C compares recombinant Apo A-I with Apo A-I purified from blood serum. It shows the degree of dissociation, α, as determined by AUC measurements at 20 and 37 °C. The data allow two conclusions. (i) Recombinant Apo A-I and serum-derived Apo A-I yield identical results within experimental error. (ii) The AUC data can be described quantitatively by the cooperative association model as displayed by the solid lines in Figure 3C. At 37 °C, the simulation yielded the following values: $K_a = 4 \times 10^5$ M^{-1}, $\sigma = 0.003$, and $n = 8$. They agree perfectly with the ITC data. At 20 °C, the AUC data predicted a K_a of 8×10^5 M^{-1}, which was slightly higher than expected on the basis of ITC measurements.

Differential Scanning Calorimetry Analysis of Apo A-I Unfolding. The thermodynamics of Apo A-I unfolding was quantified by measuring dilute solutions of Apo A-I with differential scanning calorimetry. Figure 4 shows the melting curves for Apo A-I concentrations from 0.5 to 4.5 mg/mL. The maximum of the molar heat capacity occurred at 52.6 °C (T_0) for all three samples and was independent of protein concentration. The heat of transition, ΔH_N^U, was 422 kJ/mol (101 kcal/mol) and was also independent of the protein concentration, at least at 70.9 and 160 μM as the DSC scans were superimposable within experimental error. DSC scans were fully reversible if the temperature did not exceed 75 °C. Previous work on Apo A-I yielded DSC maxima between 57 and 63 °C and melting enthalpies between 58 and 200 kcal/mol.[5,6,27] The differences may be caused by differences in protein preparations and salt conditions and also by neglecting the difference between initial and final C_p values. [In differential scanning calorimetry the sharpness of a transition is an indicator of the purity of the substance, the homogeneity of the probe, and the cooperativity of the transition. The recombinant Apo A-1 (with two additional C-terminal glycines) used here yielded the sharpest transition compared to all published DSC data on Apo A-I. A survey of DSC data of Apo A-I of different origin reveals a complex situation. Unfolding curves composed of three consecutive non-two-state transitions,[5,6] two consecutive two-state transitions,[27] or just one broad transition[12] were reported. Likewise, the unfolding enthalpy $\Delta_N^U H°$ was 200 kcal/mol,[5] 48 kcal/mol[6] (main peak), and 84 kcal/mol,[27] and estimated to be 200 kcal/mol.[12] The width of the melting curve at half-height was 14.3 °C in our measurements but ranged from 14 °C[6] (main peak) over 20 °C[27] and 22 °C[6] to 25 °C.[12] In the latter case[12] the MALDI mass of recombinant wild-type Apo A-1 is given as 29798 Da, which is 1719 Da (~14 amino acids) larger than that of authentic human Apo A-1. This could explain the differences observed in association behavior and differential scanning calorimetry between this study and ref 12.]

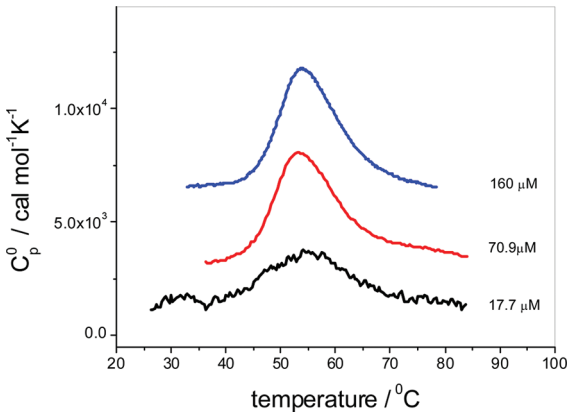

Figure 4. Differential scanning calorimetry (DSC) of recombinant Apo A-I. The Apo A-I unfolding reaction was measured at 17.7, 70.9, and 160 μM. The transition maximum occurred at 52−53 °C and was concentration-independent. The normalized DSC scans at 70.9 and 160 μM are superimposable. The heating rate was 1 °C/min. All measurements were taken in buffer [10 mM sodium phosphate, 138 mM NaCl (pH 7.4), and 0.02% NaN_3]. The measurement at 17.7 μM was at the limit of sensitivity and could not be used for an evaluation of unfolding enthalpy.

As Apo A-I unfolding was independent of protein concentration above 17 μM, the association process described in the previous section did not influence unfolding. This is discussed below in the context of a quantitative comparison of the two different equilibria.

A general problem in evaluating DSC thermograms is the definition of the baseline.[28] In these studies, the baseline was defined by the linear part of the calorimetric scan at low temperatures and was extrapolated beyond the main transition. This appeared to be justified as it led to constant C_p values before and after the transition. The difference between the two linear parts is the molar heat capacity change $\Delta_N^U C_p$ of 5.0 kJ mol^{-1} K^{-1} (1.2 kcal mol^{-1} K^{-1}). A change in $\Delta_N^U C_p$ was not reported in the earlier DSC experiments.[5,6,12,27] However, $\Delta_N^U C_p$ changes of several kilojoules per mole per kelvin are found for other proteins (e.g., T4 lysozyme, 164 amino acids, $\Delta_N^U C_p$ = 5.1 kJ mol^{-1} K^{-1};[29] human growth hormone, 192 amino acids, $\Delta_N^U C_p$ = 8 kJ mol^{-1} K^{-1}[30]).

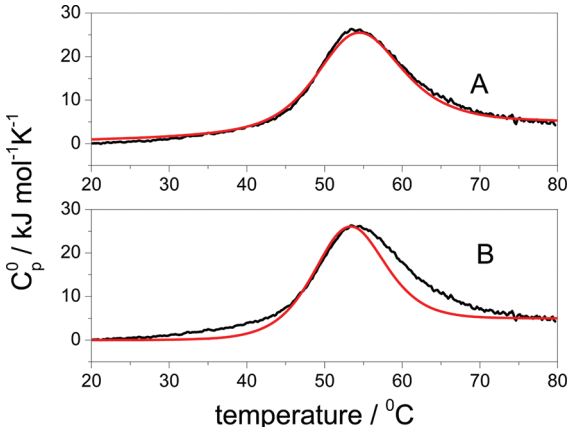

Figure 5. Interpretation of Apo A-I thermal unfolding comparing two models. The experimental result (black line) is the DSC scan of a 160 μM Apo A-I solution in PBS buffer measured at a heating rate of 1 °C/min. (A) Zimm−Bragg model (red line) using the following values: $\sigma = 4.4 \times 10^{-5}$, h = 1100 cal/mol, n = 85, and $\Delta_N^U C_p°$ = 5.0 kJ/mol. The predicted T_0 = 325.6 K. The midpoint of the h → β, rc transition of an infinitely long α-helix is at 339.7 K (T_1). (B) N ⇄ U two-state model (red line) using the following values: $\Delta_N^U H$ = 285 kJ/mol (68.2 kcal/mol), $\Delta_N^U C_p°$ = 5.0 kJ/mol, and T_0 = 325.6 K.

Knowledge of $\Delta_N^U C_p$ provides insight into the molecular nature of Apo A-I unfolding. At low temperatures (≤20 °C), amide hydrogens are well protected by hydrogen bonds in the native protein structure. This is true whether the site in question is deeply buried or at the solvent-exposed surface.[31] Hydrogen−deuterium exchange was thus used to determine the α-helical segments of Apo A-I.[31] Thermal unfolding of Apo A-I

dx.doi.org/10.1021/bi2013799 | Biochemistry 2012, 51, 1269−1280

increases the molecular fluctuations, and H-bonds are transiently broken and brought into contact with solvent. While the increase in heat capacity is generally assigned to the exposure of apolar groups, a systematic study of cyclic peptides led to the following conclusion: "The large apolar contribution suggests that a liquid hydrocarbon model of the hydrophobic effect does not accurately represent the apolar contribution to $\Delta H°$ of denaturation. Rather, significant enthalpic stabilizing contributions are found to arise from peptide groups (hydrogen bonding)."[32] The heat capacity change upon water exposure of a single amide group has been estimated ($\Delta^{U}_{N}C_p$ = 60 ± 6 J mol^{-1} K^{-1}).[32] The increase in $\Delta^{U}_{N}C_p$ of 5.0 ± 0.5 kJ mol^{-1} K^{-1} (1.22 kcal mol^{-1} K^{-1}) observed for Apo A-I could thus be caused by the exposure of ~83 amino acids, in agreement with the CD spectroscopy results to be discussed below.

Figure 5 shows the temperature dependence of the heat capacity and compares the experimental data with the predictions of the cooperative model (Figure 5A) and the N ⇄ U two-state model (Figure 5B). An improved fit of Figure 5B could be obtained by superimposing several N ⇄ U two-state transitions. Two or three N ⇄ U two-state transitions were combined to simulate previous experimental DSC data as discussed above. The increase in molar heat capacity between the fully folded and unfolded protein was not considered in these earlier analyses.

CD Spectroscopy Analysis of Thermal Apo A-I Unfolding. The structural changes associated with thermal unfolding were investigated via CD spectroscopy. Figure 6A depicts CD spectra of Apo A-I in buffer measured in 10 °C steps between 25 and 85 °C. After the sample had been heated to 85 °C and cooled to 25 °C, the CD spectrum was virtually identical to the starting spectrum illustrating the reversibility of thermal unfolding. Inspection of Figure 6A reveals spectral shapes characteristic of a predominantly α-helical structure. However, a continuous loss of α-helix structure occurs with an increase in temperature.

The quantitative evaluation of the α-helix fraction, f_h, is possible with

$$f_h = (\Theta_{222} + 3000)/-39000 \quad (31)$$

where Θ_{222} is the molar ellipticity per residue at 222 nm. The α-helix content evaluated by eq 31 decreases from 45% at 25 °C to 18% at 85 °C, consistent with earlier observations.[5−7,9,33] Surprisingly, the loss of α-helix is compensated mainly by an increase in β-structure content and not by random coil elements. This follows from simulations of the CD spectra in the range of 190−240 nm, yielding the fractions of the main structural elements as shown in Figure 6B. [Two different algorithms (cf. Materials and Methods) were applied and produced almost identical results.] The α-helix content is found to be higher than that estimated with eq 31. It is constant at ~50−54% below 45 °C and decreases to 21% at 85 °C. The loss of the α-helix fraction upon heating (Δf_h) is 33%. At the same time, the β-structure contribution increases from 26 to 50%, which has escaped notice in previous studies. The percentage of random coil segments increases modestly from 19 to 28%. The CD spectral simulations show that (i) the melting of Apo A-I is a multistate process and (ii) the spectroscopic change (Δf_h) of 33% corresponds to the loss of (243 + 2) × 0.33 = 81 helical segments. This result is in excellent agreement with the thermodynamic analysis given above (i.e., 83 helical segments) based on the change in the molar heat capacity $\Delta^{U}_{N}C_p$. The solid line through the α-helix data is the prediction of the Zimm−Bragg model.

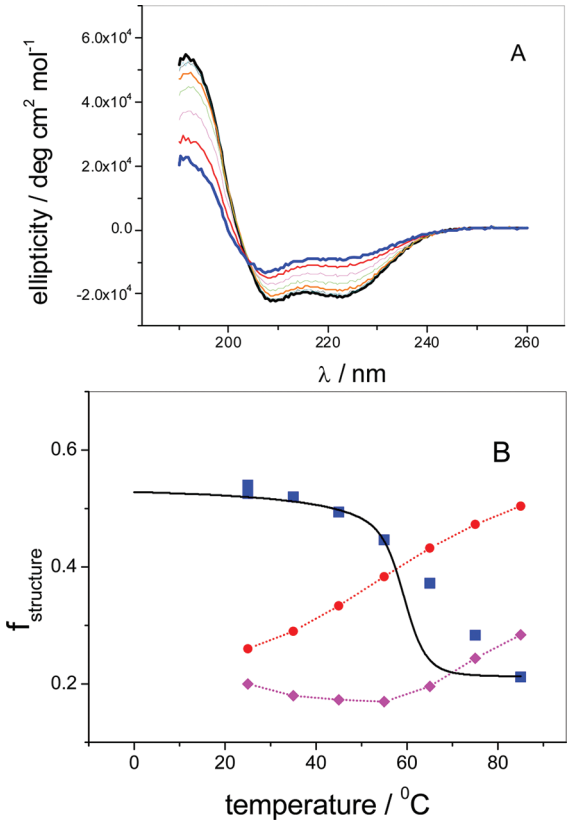

Figure 6. Thermal unfolding analysis of recombinant Apo A-I by CD spectroscopy. (A) Far-UV CD spectra of Apo A-I for temperatures between 25 °C (black line) and 85 °C (blue line) recorded in 10 °C steps. The Apo A-I concentration was 0.5 mg/mL (17.7 μM) in buffer [100 mM NaF and 10 mM sodium phosphate (pH 7.4)]. Measurements at a lower concentration of 0.1 mg/mL (3.6 μM) yielded similar spectra in the range of 25−65 °C. (B) Deconvolution of the CD spectra in terms of three structural elements: (■) α-helix, (●) β-sheet, and (◆) random coil. The β-turn element is not shown as it was always close to zero. This panel demonstrates that the loss of α-helix content is mostly compensated by an increase in β-structure content. The solid line is the predicted α-helix content as calculated with the Zimm−Bragg theory using a nucleation parameter (σ) of 4.4 × 10^{-5}, a hydrogen bond enthalpy per helix residue (h) of 1100 cal/mol, and an n of 85 as deduced from the DSC and CD unfolding experiments.

The hydrogen bond enthalpy in a β-structure is much lower than that in an α-helix. For the membrane-binding peptide $(KIGAKI)_3$, composed of 18 amino acids, h_β is 0.96 kJ/mol (0.26 kcal/mol) for breaking a hydrogen bond in long stretches ($n \geq 18$) of β-structure.[34] For shorter arrays of β-structure, h_β can be 0 kJ/mol or even slightly negative.[35] Thus, from a thermodynamic point of view, the α-helix ⇄ β-structure transition can be similar or identical to the α-helix ⇄ random coil transition, and β-elements and random coil elements will be considered as thermodynamically equivalent in this context. Significant differences between the enthalpies of β-segment and random coil segment formation should be reflected in the parameters of the Zimm−Bragg theory. However, for Apo A-I, and other proteins that we investigated, the enthalpy of helix disruption (h value used in eq 6) was always in the range of 800−1300 cal/mol.

dx.doi.org/10.1021/bi2013799 | Biochemistry 2012, 51, 1269−1280

As an aside, it should be noted that a plot of the λ = 222 nm ellipticity versus temperature (data of Figure 6A) has its midpoint at 61 °C, which is 8 °C higher than the T_0 of the caloric transition. The discrepancy between CD spectroscopy and DSC is also obvious from inspection of Figure 6B. CD spectroscopy monitors changes in secondary structure only, while DSC includes also the melting of the tertiary structure.

DISCUSSION

This analysis is of general relevance for the understanding of the thermodynamic behavior of oligomeric systems. Our experimental and theoretical results shed light on two different problems, that is, (i) the thermodynamics of unfolding an α-helical protein and (ii) the temperature and concentration dependence of a monomer ⇄ oligomer equilibrium. Cooperativity was found to play an essential role in both processes. The Zimm−Bragg theory was introduced as an alternative to the classical N ⇄ U two-state model for a consistent analysis of calorimetric and spectroscopic data for Apo A-I unfolding. The isodesmic self-association model was employed to describe the oligomerization of Apo A-I. The free energy for the addition of a monomer to any oligomer was assumed to be constant, but the initial dimerization was less favorable by the nucleation factor σ, introducing cooperativity. Maximal self-association occurred at 21 °C, whereas the midpoint of unfolding was at 52.6 °C. The measured heat of unfolding was ∼100 kcal/mol and by a factor of 5−10 larger than the heat of self-association. The unfolding enthalpy was independent of concentration up to 160 μM. In the following, we compare the temperature course of unfolding with that of Apo A-I dissociation. We provide a model calculation for the temperature and concentration depencence of C_p° for a cooperative monomer ⇄ oligomer equilibrium.

Thermodynamics of Apo A-I Unfolding. Crystal structure[3] and protein sequence analysis[36] predict that the Apo A-I region between residues 44 and 241 is largely α-helical. The 2.2 Å crystal structure of C-terminally truncated Apo A-I (184 N-terminal residues) reveals an approximate half-circle (80% helix) with the N-terminus arranged in a loose bundle composed of four helices and an extended segment.[3] Unfolding of Apo A-I corresponds essentially to a disruption of α-helical regions and, to a minor extent, to the unfolding of the four-helix tertiary structure. As a new approach, we describe Apo A-I unfolding with the cooperative Zimm−Bragg theory. Figure 5A compares the experimental DSC scan with the prediction of the cooperative h ⇄ β, random coil model. The following parameters were used: H-bond stability h = 4.6 kJ/mol (1100 cal/mol), nucleation factor $\sigma = 4.4 \times 10^{-5}$, T_1 = 339.7 K, and n = 85. The predicted midpoint temperature for this short α-helix was 325.6 K, in agreement with the maximum of the measured C_p versus T curve. Attempts to simulate the DSC curves with chain lengths distinctly shorter than n = 85 were unsuccessful as the width of the transition region became too broad. Hydrogen exchange experiments indicate long stretches of α-helix secondary structure between Apo A-1 residues 7 and 115 with a total of 95 α-helical residues.[31] It is the unfolding of this region that is most likely monitored in the DSC experiment. A second α-helical region of 32 residues is found at positions 147−178.[31] As Apo A-1 has an α-helical content of 18% even at 85 °C (corresponding to ∼40 residues), this α-helix could account for the residual ellipticity observed via CD spectroscopy (cf. Figure 6).

The enthalpy per hydrogen bond can also be derived directly from the transition enthalpy without resorting to a particular model. As the unfolding enthalpy ($\Delta_N^U H$) is 422 kJ/mol (101 kcal/mol) and as CD spectroscopy suggests that ∼85 segments are involved in the transition, an α-helix stability (h) of 422/85 ≈ 5.0 kJ/mol (1188 cal/mol) can be estimated, in good agreement with the value used in Zimm−Bragg theory.

Figure 5B displays the related calculations for the N ⇄ U model. The experimental transition temperature (T_0) was 325.6 K, as defined by the maximum of the C_p curve. The unfolding enthalpy $\Delta_N^U H$ required for an optimal fit was 285 kJ/mol (68.2 kcal/mol). This value is much lower than the experimental result of 422 kJ/mol (101 kcal/mol). The N ⇄ U model also predicts a transition sharper than that observed experimentally.

The theoretical transition enthalpy characterizing the two-state N ⇄ U equilibrium is often denoted with van't Hoff enthalpy, ΔH_{vH}, and derived from CD measurements. For Apo A-I, ΔH_{vH} is much smaller than the calorimetric transition enthalpy, $\Delta_N^U H^\circ$, and a $\Delta H_{vH}/\Delta_N^U H^\circ$ ratio of <1 is considered to reflect the low cooperativity of Apo A-I unfolding.[5,6,27] In contrast, a high cooperativity index (n_{coop}) of 7.8 was defined by applying the Hill equation to describe the sigmoidicity of the thermal denaturation curve.[7] The Zimm−Bragg theory finally describes cooperativity in terms of the steepness of the transition curve. The smaller the nucleation parameter σ and the larger the number of hydrogen bonds to be broken, the more cooperative the transition and the steeper the transition curve. In terms of the Zimm−Bragg theory, Apo A-I unfolding is a highly cooperative process.

Thermodynamics of Apo A-I Self-Association and Monomer−Oligomer Probabilities. Both AUC and ITC demonstrate that self-association of Apo A-I is a concentration-dependent process. Figure 3B indicates that Apo A-I is monomeric below ∼3 μM and self-associates at higher concentrations. The cooperative association model with an n of 8 and a σ of 0.003 gave the best fit to both the ITC and AUC data. Knowledge of K_a as deduced from the dissociation isotherm permits the calculation of the free energy, ΔG_a°, and entropy $T\Delta S_a^\circ$ (see Table 1). At room temperature, the enthalpy of association, ΔH_a°, is close to zero while the Gibbs free energy, ΔH_a°, is large and negative. This means that the entropy of association is large and positive and is the driving force for the association below 20 °C. As the temperature increases, the reaction becomes exothermic and the contribution of entropy gradually decreases.

The Apo A-I solution contains states of oligomerization 1, 2, ..., and j. The probability of their occurrence can be calculated with the partition function Q. If p_j is defined as the probability of j-mers in solution, i.e., the number of oligomers of size j divided by the total number of species in solution, then

$$p_j = \frac{n_j}{\sum_j n_j} \tag{32}$$

For the cooperative model, one finds

$$p_1 = Q^{-1} \text{ and } p_j = \sigma(K_a c_A)^{j-1}/Q \tag{33}$$

Figure 7 provides a comparison of the fraction of monomers, p_1, and octamers, p_8, plotted versus the total monomer concentration c_A^0 (maximal association number n = 8). Also included are the degree of dissociation α (=c_A/c_A^0) and the

dx.doi.org/10.1021/bi2013799 | Biochemistry 2012, 51, 1269−1280

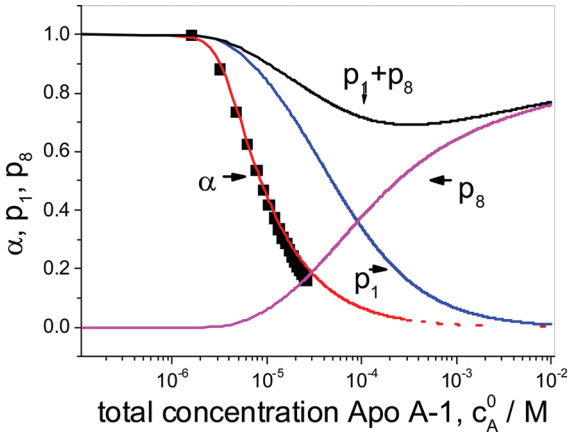

Figure 7. Self-association of Apo A-I. Probabilities of monomers and octamers. (■) Degree of dissociation of Apo A-I, α, as derived from the ITC experiment shown in Figure 1. Solid lines show the predicted probabilities (mole fractions) of monomers, p_1, and octamers, p_8, as a function of the total protein monomer concentration, c_A^0, at 40 °C . Calculations with the cooperative association model: σ = 0.003, K_a = 3.5 × 10^5 M^{-1}, and maximal association number n = 8.

experimental results for α obtained from the titration experiment shown in Figure 1.

Figure 7 reveals that the degree of dissociation, α, decreases faster than the monomer probability, p_1. This follows because only one A_8 molecule is generated when eight monomers associate, and the loss of monomers thus proceeds faster than the growth in the number of oligomers. Monomers and octamers are the predominant species in solution. However, the sum p_1 + p_8 goes through a minimum at a total Apo A-I concentration of ~6.7 × 10^{-4} M, with monomers and octamers accounting for only 70% of the total species. This indicates that the solution contains additional intermediates.

Earlier studies of Apo A-I self-association primarily relied on AUC measurements in which a monomer−dimer−tetramer−octamer model was assumed.[22,23] Separate association constants were defined for each association step. However, when applied to our ITC data, this model did not provide satisfactory quantitative results.

Apo A-I association has also been reported in terms of an apparent molecular mass.[26] M_{app} can be calculated in this notation as

$$M_{app} = \sum_{j=1}^{n} j p_j M_W^A \qquad (34)$$

where M_W^A is the molecular mass of the Apo A-I monomer. Equation 34 was used to simulate the data in Figure 3B. Excellent agreement with the ITC experiments was obtained.

We have also analyzed previous M_{app} values for Apo A-I with the cooperative model discussed above. For example, simulating the M_{app} data given in ref 26 (Figure 2, 0.13 M KCl) with the cooperative model required a σ of 0.003 and a K of 6 × 10^5 M^{-1} for an n of 8. These are exactly the values predicted by our ITC experiments for the self-association at 20 °C.

Apo A-I Unfolding versus Apo A-I Dissociation. Protein association and denaturation can be tightly connected processes as demonstrated for a 54-amino acid fragment of GCN4.[37] Increasing the protein concentration by a factor of 100 in this example shifts the midpoint of the unfolding transition by ~20 °C to higher temperatures. In contrast, Apo A-I unfolding was independent of the protein concentration (up to 160 μM). The level of self-association reached its maximum at 21 °C and decreased at both lower and higher temperatures, while Apo A-I unfolding had its maximal change in heat capacity (midpoint of the unfolding transition) at 52.6 °C. Considering a 160 μM (70.7 μM) Apo A-I solution at 45 °C, which is the onset temperature of the unfolding reaction, the fraction of monomers is 6.5% (12.8%), while that of octamers is 59% (51%), referenced to total monomeric Apo A-I. Hence, at the beginning of the unfolding process, the solution is mainly composed of oligomers. We therefore calculated the contribution of dissociation of Apo A-I to the molar heat capacity change by the following thought experiment. We considered an Apo A-I solution where the Apo A-I molecules were locked in their native conformation at all temperatures. The change in molar heat capacity was thus exclusively caused by the dissociation of Apo A-I complexes. Using eqs 19, 20, and 22, the molar heat capacity change of the dissociation equilibrium was calculated and compared with that of protein unfolding. Figure 8 displays

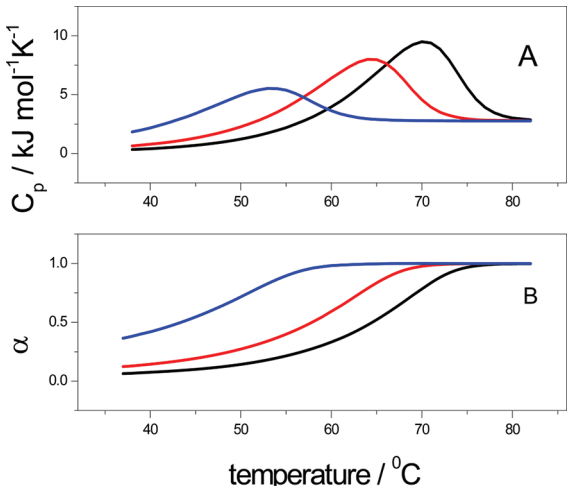

Figure 8. Computed DSC scans for a solution containing virtual Apo A-I oligomers that dissociate but remain folded. Three different protein concentrations were compared. The melting curves were calculated with the cooperative association model. The temperature dependence of the association constant was ΔH_a (kilocalories per mole) = −0.659(T − 273) + 13.288, and the association constant at 273 K was 3.5 × 10^5 M^{-1}. The temperature dependence of K_a was identical to that in Figure 5B. The maximal association number (n) is 8, and the cooperativity parameter (σ) is 0.003. The blue line is for 17.7 μM, the red line for 70.7 μM, and the magenta line for 160 μM. (A) Molar heat capacity change, $C_p°$. The maximum of the dissociation reaction shifts to higher temperatures with an increase in protein concentration. (B) Degree of dissociation, α.

such calculations for three protein concentrations. As expected, the heat capacity of the dissociation equilibrium depended on the total Apo A-I concentration, c_A^0. The maximum of the molar heat capacity shifted from 55 °C at 17 μM Apo A-I to 72 °C at 160 μM, while the width of the transition was reduced. The predicted molar heat capacity was 3.7 kJ mol^{-1} K^{-1} (1.98 kJ mol^{-1} K^{-1}) for 70 μM (160 μM) Apo A-I at 53 °C, which was much smaller than the molar heat capacity at the maximal C_p of the unfolding reaction ($C_p°$ = 24.6 kJ mol^{-1} K^{-1}). Figure 8 predicts that the dissociation of virtual, folded Apo A-I complexes should occur at temperatures higher than that of Apo A-I unfolding. An additional transition peak should appear

dx.doi.org/10.1021/bi2013799 | Biochemistry 2012, 51, 1269−1280

in the C_p versus T diagram. As this was not observed experimentally, it is safe to conclude that Apo A-I unfolding and dissociation occur simultaneously. This is consistent with the observed concentration independence of the unfolding transition. As the heat capacity change of the dissociation reaction makes only a small contribution (figure 8), the calorimetric $\Delta_N^U H$ is dominated by the unfolding of secondary structural elements.

Concluding Remarks. We showed that protein self-association can be readily analyzed by the method of binding partition functions. This approach allowed comparison of different association models and provided analytic expressions for analysis of experimental AUC and ITC results. The thermodynamic parameters of Apo A-I self-association are quite similar to those of other, more specific, protein−protein interactions. For example, the interaction of stathmin, a 17 kDa protein, with tubulin (~55 kDa) was investigated with ITC.[38] Similar to these results, the binding constants of the binary complex equaled 10^6−10^7 M^{-1}. Likewise, $\Delta H°$ was also endothermic at low temperatures and reached zero at 28 °C. The fact that some biological systems have very small reaction enthalpies at ambient temperature demonstrates that they minimize the temperature sensitivity of the corresponding chemical equilibria, leading to temperature-independent concentrations of the involved proteins. Another example supporting this conclusion is apolipoprotein C-1 showing a maximum of self-association at room temperature that is also reduced upon heating or cooling.[39]

We further showed that the cooperative Zimm−Bragg model provided an accurate description of Apo A-I unfolding and should be considered as an alternative to the common two-state N ⇄ U model, at least for proteins with a high α-helix content. For comparison, we analyzed experimental DSC results for a 22 kDa (N-terminal) fragment of Apo E2 that is ~50% α-helical at 20 °C[40] (Figure 1 of ref 40). An excellent fit of the DSC curve was obtained with an h of 5.02 kJ/mol (1200 cal/mol) and a σ of 3×10^{-5}, parameters very similar to those of Apo A-I (data not shown). As a second example, we analyzed the calorimetric trace of a 50-residue peptide (Figure 3 of ref 18) with the Zimm−Bragg model and again obtained excellent agreement with experimental values using an h of 930 cal/mol and a σ of 4×10^{-3} (data not shown). These results are consistent with a follow-up study of the same peptide with CD spectroscopy resulting in an h of 960 ± 20 cal/mol and a σ of $(2.9 \pm 0.3) \times 10^{-3}$.[41] Application of the N ⇄ U model completely failed for this 50-residue peptide.

AUTHOR INFORMATION

Corresponding Author

*Telephone: +41-61-267 2190. Fax: +41-61-267 2189. E-mail: joachim.seelig@unibas.ch.

Funding

Supported by Swiss National Science Foundation Grant 31003A-129701.

Notes

The authors declare no competing financial interest.

ACKNOWLEDGMENTS

We are indebted to Dr. Francis Müller and Eric André Kusznir (Roche) for providing the AUC data for Figure 3C. We are grateful to Howard Etlinger for carefully reading the manuscript and valuable comments.

REFERENCES

(1) Segrest, J. P., Li, L., Anantharamaiah, G. M., Harvey, S. C., Liadaki, K. N., and Zannis, V. (2000) Structure and function of apolipoprotein A-I and high-density lipoprotein. *Curr. Opin. Lipidol. 11*, 105−115.

(2) Frank, P. G., and Marcel, Y. L. (2000) Apolipoprotein A-I: Structure-function relationships. *J. Lipid Res. 41*, 853−872.

(3) Mei, X., and Atkinson, D. (2011) Crystal structure of C-terminal truncated apolipoprotein A-I reveals the assembly of high density lipoprotein (HDL) by dimerization. *J. Biol. Chem. 286*, 38570−38582.

(4) Borhani, D. W., Rogers, D. P., Engler, J. A., and Brouillette, C. G. (1997) Crystal structure of truncated human apolipoprotein A-I suggests a lipid-bound conformation. *Proc. Natl. Acad. Sci. U.S.A. 94*, 12291−12296.

(5) Gursky, O., and Atkinson, D. (1996) Thermal unfolding of human high-density apolipoprotein A-1: Implications for a lipid-free molten globular state. *Proc. Natl. Acad. Sci. U.S.A. 93*, 2991−2995.

(6) Suurkuusk, M., and Hallen, D. (1999) Denaturation of apolipoprotein A-I and the monomer form of apolipoprotein A-I_{Milano}. *Eur. J. Biochem. 265*, 346−352.

(7) Saito, H., Dhanasekaran, P., Nguyen, D., Holvoet, P., Lund-Katz, S., and Phillips, M. C. (2003) Domain structure and lipid interaction in human apolipoproteins A-I and E, a general model. *J. Biol. Chem. 278*, 23227−23232.

(8) Silva, R. A., Hilliard, G. M., Fang, J., Macha, S., and Davidson, W. S. (2005) A three-dimensional molecular model of lipid-free apolipoprotein A-I determined by cross-linking/mass spectrometry and sequence threading. *Biochemistry 44*, 2759−2769.

(9) Arnulphi, C., Jin, L., Tricerri, M. A., and Jonas, A. (2004) Enthalpy-driven apolipoprotein A-I and lipid bilayer interaction indicating protein penetration upon lipid binding. *Biochemistry 43*, 12258−12264.

(10) Silva, R. A., Huang, R., Morris, J., Fang, J., Gracheva, E. O., Ren, G., Kontush, A., Jerome, W. G., Rye, K. A., and Davidson, W. S. (2008) Structure of apolipoprotein A-I in spherical high density lipoproteins of different sizes. *Proc. Natl. Acad. Sci. U.S.A. 105*, 12176−12181.

(11) Swaney, J. B. (1983) Reconstitution of apolipoprotein A-I from human high density lipoprotein with bovine brain sphingomyelin. *J. Biol. Chem. 258*, 1254−1259.

(12) Jayaraman, S., Abe-Dohmae, S., Yokoyama, S., and Cavigiolio, G. (2011) Impact of self-association on function of apolipoprotein A-I. *J. Biol. Chem. 286*, 35610−35623.

(13) Sreerama, N., and Woody, R. W. (2004) On the analysis of membrane protein circular dichroism spectra. *Protein Sci. 13*, 100−112.

(14) Reed, J., and Reed, T. A. (1997) A set of constructed type spectra for the practical estimation of peptide secondary structure from circular dichroism. *Anal. Biochem. 254*, 36−40.

(15) Zimm, B. H., and Bragg, J. K. (1959) Theory of the phase transition between helix and random coil in polypeptide chains. *J. Chem. Phys. 31*, 526−535.

(16) Chou, P. Y., and Scheraga, H. A. (1971) Calorimetric measurement of enthalpy change in the isothermal helix−coil transition of poly-L-lysine in aqueous solution. *Biopolymers 10*, 657−680.

(17) Rialdi, G., and Hermans, J. Jr. (1966) Calorimetric heat of the helix-coil transition of poly-L-glutamic acid. *J. Am. Chem. Soc. 88*, 5719−5720.

(18) Scholtz, J. M., Marqusee, S., Baldwin, R. L., York, E. J., Stewart, J. M., Santoro, M., and Bolen, D. W. (1991) Calorimetric determination of the enthalpy change for the α-helix to coil transition of an alanine peptide in water. *Proc. Natl. Acad. Sci. U.S.A. 88*, 2854−2858.

(19) Davidson, N. (1962) *Statistical Mechanics*, pp 385, McGraw-Hill, New York.

(20) Beck, A., Li-Blatter, X., Seelig, A., and Seelig, J. (2010) On the interaction of ionic detergents with lipid membranes. Thermodynamic comparison of n-alkyl-$^+N(CH_3)_3$ and n-alkyl-SO_4^-. *J. Phys. Chem. B 114*, 15862−15871.

(21) Wyman, J., and Gill, S. J. (1990) *Binding and Linkage. Functional chemistry of biological macromolecules*, University Science Books, Mill Valley, CA.
(22) Vitello, L. B., and Scanu, A. M. (1976) Studies on human serum high density lipoproteins. Self-association of apolipoprotein A-I in aqueous solutions. *J. Biol. Chem. 251*, 1131−1136.
(23) Swaney, J. B., and O'Brien, K. (1978) Cross-linking studies of the self-association properties of apo-A-I and apo-A-II from human high density lipoprotein. *J. Biol. Chem. 253*, 7069−7077.
(24) Heerklotz, H., and Seelig, J. (2000) Titration calorimetry of surfactant-membrane partitioning and membrane solubilization. *Biochim. Biophys. Acta 1508*, 69−85.
(25) Privalov, P. L., and Gill, S. J. (1989) The hydrophobic effect: A reappraisal. *Pure Appl. Chem. 61*, 1097−1104.
(26) Formisano, S., Brewer, H. B. Jr., and Osborne, J. C. Jr. (1978) Effect of pressure and ionic strength on the self-association of Apo-A-I from the human high density lipoprotein complex. *J. Biol. Chem. 253*, 354−359.
(27) Brouillette, C. G., Dong, W. J., Yang, Z. W., Ray, M. J., Protasevich, I. I., Cheung, H. C., and Engler, J. A. (2005) Forster resonance energy transfer measurements are consistent with a helical bundle model for lipid-free apolipoprotein A-I. *Biochemistry 44*, 16413−16425.
(28) Privalov, P. L., and Dragan, A. I. (2007) Microcalorimetry of biological macromolecules. *Biophys. Chem. 126*, 16−24.
(29) Carra, J. H., Murphy, E. C., and Privalov, P. L. (1996) Thermodynamic effects of mutations on the denaturation of T4 lysozyme. *Biophys. J. 71*, 1994−2001.
(30) Kasimova, M. R., Milstein, S. J., and Freire, E. (1998) The conformational equilibrium of human growth hormone. *J. Mol. Biol. 277*, 409−418.
(31) Chetty, P. S., Mayne, L., Lund-Katz, S., Stranz, D., Englander, S. W., and Phillips, M. C. (2009) Helical structure and stability in human apolipoprotein A-I by hydrogen exchange and mass spectrometry. *Proc. Natl. Acad. Sci. U.S.A. 106*, 19005−19010.
(32) Murphy, K. P., and Gill, S. J. (1991) Solid model compounds and the thermodynamics of protein unfolding. *J. Mol. Biol. 222*, 699−709.
(33) Saito, H., Dhanasekaran, P., Nguyen, D., Deridder, E., Holvoet, P., Lund-Katz, S., and Phillips, M. C. (2004) α-Helix formation is required for high affinity binding of human apolipoprotein A-I to lipids. *J. Biol. Chem. 279*, 20974−20981.
(34) Meier, M., and Seelig, J. (2007) Thermodynamics of the coil ⇆ β-sheet transition in a membrane environment. *J. Mol. Biol. 369*, 277−289.
(35) Meier, M., and Seelig, J. (2008) Length dependence of the coil ⇆ β-sheet transition in a membrane environment. *J. Am. Chem. Soc. 130*, 1017−1024.
(36) Nolte, R. T., and Atkinson, D. (1992) Conformational analysis of apolipoprotein A-I and E-3 based on primary sequence and circular dichroism. *Biophys. J. 63*, 1221−1239.
(37) Thompson, K. S., Vinson, C. R., and Freire, E. (1993) Thermodynamic characterization of the structural stability of the coiled-coil region of the bZIP transcription factor GCN4. *Biochemistry 32*, 5491−5496.
(38) Honnappa, S., Cutting, B., Jahnke, W., Seelig, J., and Steinmetz, M. O. (2003) Thermodynamics of the Op18/stathmin-tubulin interaction. *J. Biol. Chem. 278*, 38926−38934.
(39) Gursky, O., and Atkinson, D. (1998) Thermodynamic analysis of human plasma apolipoprotein C-1: High-temperature unfolding and low-temperature oligomer dissociation. *Biochemistry 37*, 1283−1291.
(40) Acharya, P., Segall, M. L., Zaiou, M., Morrow, J., Weisgraber, K. H., Phillips, M. C., Lund-Katz, S., and Snow, J. (2002) Comparison of the stabilities and unfolding pathways of human apolipoprotein E isoforms by differential scanning calorimetry and circular dichroism. *Biochim. Biophys. Acta 1584*, 9−19.
(41) Scholtz, J. M., Qian, H., York, E. J., Stewart, J. M., and Baldwin, R. L. (1991) Parameters of helix-coil transition theory for alanine-based peptides of varying chain lengths in water. *Biopolymers 31*, 1463−1470.